ELSEVIER

Journal of Electron Spectroscopy and Related Phenomena 86 (1997) 175–183

JOURNAL OF ELECTRON SPECTROSCOPY and Related Phenomena

Bioinorganic applications of X-ray multiplets — The impact of Theo Thole's work

Stephen P. Cramer[a,*], Corie Y. Ralston[a], Hongxin Wang[b], Craig Bryant[b]

[a]*Department of Applied Science, University of California, Davis, CA 95616, USA*
[b]*Lawrence Berkeley National Laboratory, Berkeley, CA 94720, USA*

Abstract

Prior to the work of Theo Thole and his collaborators, the vast majority of biological X-ray spectroscopy involved either EXAFS or hard X-ray XANES spectroscopy. Theo Thole's ligand field multiplet theory revealed the rich information content of transition metal L-edges, and it helped prompt the first measurements on metalloproteins. His contributions to XMCD also prompted the first low-temperature/high-field experiments on paramagnetic centers in proteins. This paper describes some recent work in biological soft X-ray spectroscopy that was stimulated by Thole's findings. Representative Ni protein absorption spectra are shown, illustrating detection of Ni(I), Ni(III), and high- and low-spin Ni(II) in Ni hydrogenase and CO dehydrogenase. New XMCD spectra for Cu in plastocyanin and Fe in a 2Fe ferredoxin are presented. The exciting prospects for soft X-ray absorption and XMCD of metalloproteins are summarized. © 1997 Elsevier Science B.V.

Keywords: Ni enzymes, hydrogenase; CO dehydrogenase; Ni L-edges; X-ray magnetic circular dichroism

1. Introduction

The theoretical insights that Theo Thole brought to X-ray spectroscopy prompted a number of experiments on bioinorganic samples. In this article we first discuss some of the experimental hurdles to conducting soft X-ray absorption and MCD experiments on metalloproteins. We then report results on fluorescence-detected soft X-ray absorption spectroscopy of Ni proteins, where the Thole ligand field multiplet approach helps exploit the rich information content of this region. We also report soft X-ray magnetic circular dichroism (XMCD) measurements on paramagnetic metals in proteins that were stimulated by Thole's predictions and sum rules. We conclude with some speculation on future directions for bioinorganic soft X-ray spectroscopy.

The reasons for interest in the soft X-ray region can be summarised as: 1) resolution, 2) selection rules, 3) multiplets and 4) magnetic circular dichroism [1]. Compared to hard X-ray K-levels, with linewidths of 1–2 eV, the intrinsic linewidths of L-levels are much narrower (300–700 meV). L-edge spectra measure dipole-allowed 2p → 3d transitions, while at the K-edge the 1s → 3d transition is a weak quadrupole process (sometimes enhanced by p–d mixing). Thanks to 2p–3d Coulomb and exchange interactions, L-edges show multiplet structure that is sensitive to the metal oxidation and spin states. Finally, because of 2p level spin–orbit coupling, L-edges also have much larger potential XMCD effects than K-edges. The net result of these factors is illustrated in

* Corresponding author.

PII S0368-2048(97)00064-9

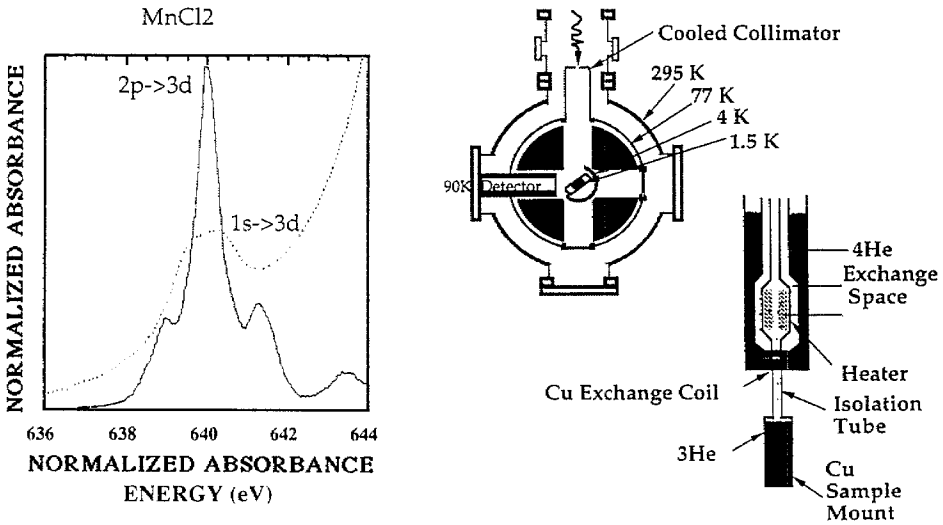

Fig. 1. (Left) Comparison of K and L edges for $MnCl_2$. (Right) Schematic of apparatus for fluorescence detected soft X-ray absorption and XMCD experiments. The most recent instrument replaces the ^{3}He cryostat with a dilution refrigerator.

Fig. 1, where the K and L edges of MnCl2 are compared.

2. Experimental aspects

Although Thole's work in ligand field multiplet theory made it clear that biological soft X-ray absorption and XMCD spectra would be informative [1,2], there were a number of experimental hurdles to overcome. The first involved protein spectroscopy under UHV conditions. The cross sections for absorption of soft X-rays are very large, hence the distances travelled through matter are very small. For example, at the Fe L-edge the path length in water only 1.0 μm. Extremely thin windows and UHV conditions are required throughout the experimental apparatus. Although this is common for surface science experiments, the conditions are not routine for biochemical samples. We have successfully made dried films of many protein samples, but there is always the danger that a protein will denature during this process, and each sample has to be checked for activity afterwards.

The second fundamental difficulty is that the metal concentration in the samples is very low, about 100–1000 p.p.m. Even though fluorescence yields are less than 1%, fluorescence detection is still the most sensitive way to enhance the metal signal. Good energy resolution is need to resolve the oxygen Kα background from the metal fluorescence signal. We are using a windowless 30-element Ge detector to capture the maximum amount of the fluorescence possible.

Finally, XMCD measurements of paramagnetic systems require both high magnetic fields and low temperatures to achieve significant sample magnetization. Since very high magnetic fields can interfere with the performance of the solid state detector, for many experiments it is preferable to go to very low temperatures. We are now using a dilution refrigerator to cool the sample, and a 2 T split coil magnet to magnetize the sample. The 3 in diameter 30-element Ge detector enters from one side, while samples are introduced through a load lock from the other side. Thin aluminum windows help reduce the heat load on the sample, allowing us to achieve ~300 mK The instrument is shown schematically in Fig. 1.

3. Ni L-edge spectroscopy

Ni L-edges are especially useful for the characterisation of this metal in biological systems. Although electron paramagnetic resonance is also a powerful tool for understanding metals in proteins, it

does not unambiguously assign oxidation states. There have often been controversies about whether signals represent Ni(I) or Ni(III) [3,4]. Also, many Ni species do not exhibit EPR signals. Low-spin Ni(II), for example, is diamagnetic, and although high-spin Ni(II) is $S = 1$, it often has very large zero field splittings that preclude EPR measurements. In this section we illustrate some of the issues surrounding two important Ni enzymes, hydrogenase and CO dehydrogenase, and we show how L-edge spectroscopy can provide complementary information to magnetic resonance, K-edge absorption, and crystallography.

4. The biochemical issues

NiFe hydrogenases catalyse the oxidation and formation of molecular hydrogen and contain a single Ni site as well as several different Fe–S clusters [4]. The NiFe hydrogenase from *D. gigas* is an $\alpha\beta$ heterodimer containing two Fe_4S_4 clusters, an Fe_3S_4 cluster, as well as a NiFe centre. Recent crystallographic data on the *D. gigas* enzyme reveals a 5-coordinate Ni site, bridged through sulphur ligands to an unusual Fe species [5] which may in fact have CO and CN ligands. The remaining centres are more conventional Fe–S clusters, arranged in a linear fashion to transfer electrons to the NiFe active site.

Carbon monoxide dehydrogenase from *Clostridium thermoaceticum* is a nickel-containing enzyme which catalyses acetyl-CoA synthesis and CO oxidation at two separate Ni sites, Centres A and C, respectively [3]. Carbon monoxide dehydrogenase from *Rhodospirillum rubrum* catalyses only CO oxidation. Since both enzymes exhibit complex EPR signals that never integrate to one spin per Ni, there is evidence for heterogeneity in the types of Ni present.

One of the key issue surrounding hydrogenase is the oxidation states involved in the characteristic states of the enzyme [4]. As shown in Scheme 1, the enzyme can exist in many forms, some of which are EPR-active, while others are EPR-silent. For the enzyme forms (from left to right), some have proposed oxidation state assignments of Ni(III) → Ni(II) → Ni(I) → Ni(0), while others favour Ni(III) → Ni(II) → Ni(III) → Ni(II) or even ligand-based redox activity.

For CO dehydrogenase, the redox and spin state assignments are just as ambiguous [3]. The situation is even more complicated because there are two types of Ni sites, Ni–A and Ni–C, and because the EPR signals arise from magnetically-coupled centres involving both Ni and Fe contributions.

5. Model compound trends

Although proper ligand field multiplet calculations are the best approach for a detailed understanding of Ni L-edges, in many cases a qualitative understanding can be had from comparison with model compounds. It is found that both Ni(I) and low-spin Ni(II) have relatively sharp L_3 and L_2 edges, in part because there is only a single vacant d-orbital. High-spin Ni(II) and Ni(III) will have at least 2 nondegenerate d-orbital vacancies, and therefore broader L-edges (Fig. 2). Also, as the oxidation state increases, the centroid of the L_3 edge moves to higher energy. A final

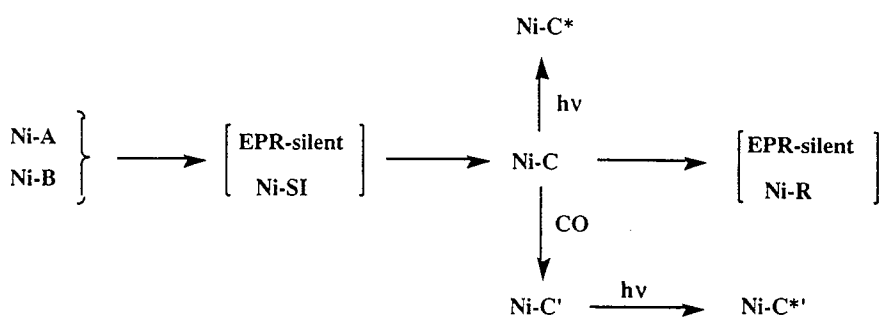

Scheme 1. Interconversion of the different forms of *D. gigas* hydrogenase.

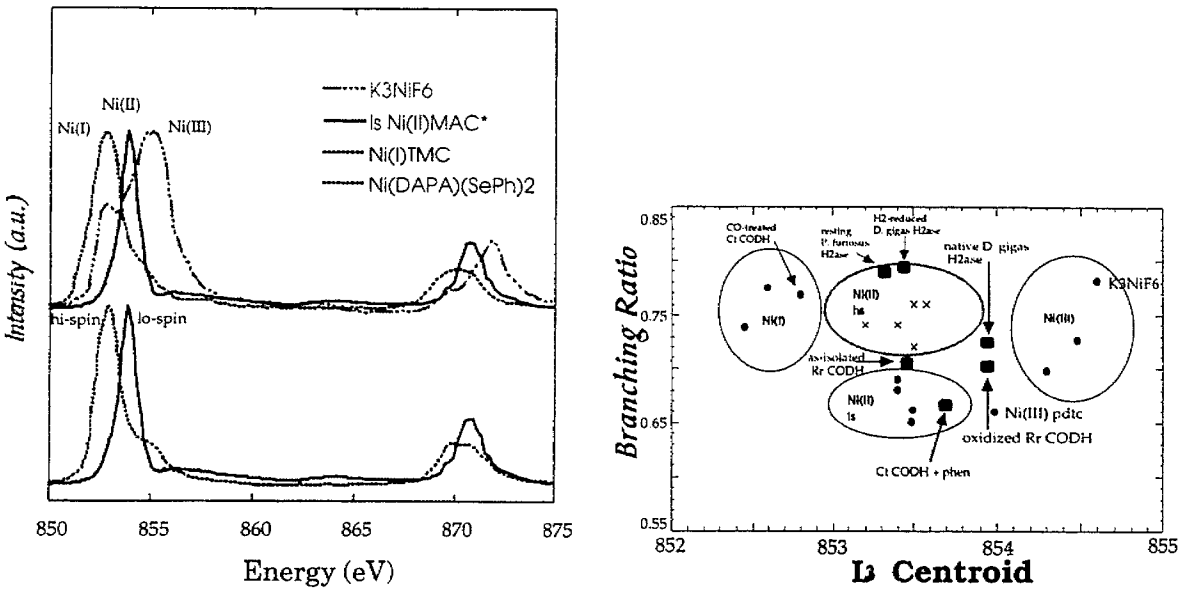

Fig. 2. (Left) Representative Ni spectra for different oxidation states and spin states. (Right) Correlation diagram for model compounds and Ni proteins.

characteristic is the ratio of L_2 to L_3 intensity. As pointed out by Thole and van der Laan [6], the L_2 intensity will be higher for low-spin complexes. The $L_2/(L_3 + L_2)$ 'branching ratio' and L_3 centroid can be combined to create a 2-dimensional diagram of characteristic spectral properties, as shown in Fig. 2. By reference to this model data as well as theoretical calculations, likely Ni spin and oxidation states can be assigned to different protein samples.

6. Application to hydrogenase and CO dehydrogenase

Representative L-edges for hydrogenase and CO dehydrogenase are shown in Fig. 3. The multiplet structure evident in the *D. baculatus* hydrogenase spectrum makes it especially easy to identify this sample as high-spin Ni(II), consistent with its position in the correlation diagram. This seems to contradict

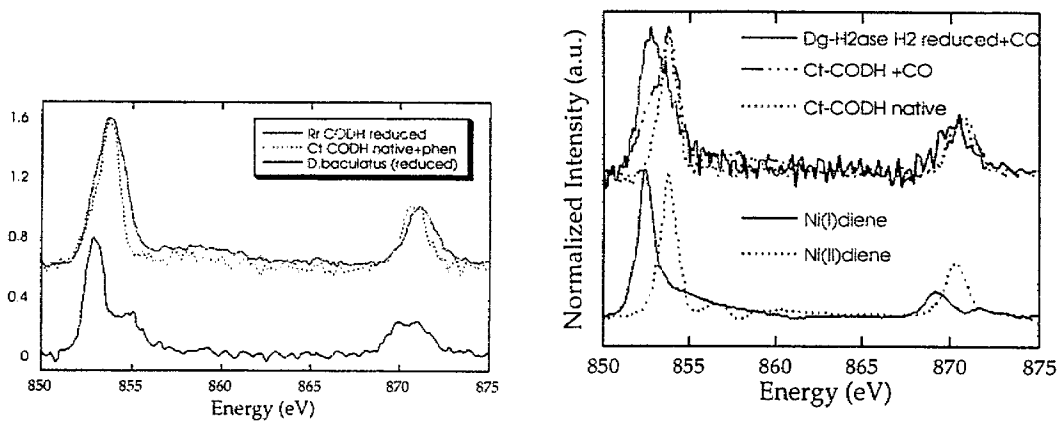

Fig. 3. (Left) L-edge spectrum for (top) *R. rubrum* and *C.* thermoaceticum CODH and (bottom) *D. baculatus* hydrogenase. (Right) CO-treated CODH (–···–···) compared with native enzyme (·····) and CO-treated hydrogenase (————————) and Ni(I) and Ni(II) model compounds.

previous magnetic susceptibility data which had identified the site as diamagnetic [7]. In contrast, the relatively strong and sharp L-edges for the CODH spectra provide evidence for predominantly low-spin Ni(II) species. Finally, both hydrogenase and CODH spectra change with the introduction of CO, in a manner consistent with formation of Ni(I) species. In other work, we have seen evidence for covalent Ni(III) species in these enzymes [8], hence all four regions of the correlation diagram have been covered.

7. XMCD of Paramagnetic metals in proteins

Thole was also a pioneer in developing the theory of X-ray magnetic circular dichroism [9–11]. This technique is attractive for bioinorganic applications for many reasons: 1) selectivity for paramagnetic species — diamagnetic species will have negligible XMCD; 2) sum rules — information about L_Z and S_Z; 3) information about spin coupling; 4) sharper features — better resolution of mixtures. Since bioinorganic samples often tend to contain mixtures of species, the prospect of selectively examining the electronic structure of different species is quite exciting. Here, we illustrate some preliminary results that illustrate the potential of bioinorganic XMCD and also raise some interesting questions.

8. Plastocyanin blue copper and other mononuclear systems

The blue copper site in plastocyanin is an ideal candidate for bioinorganic XMCD measurements and sum rule analysis. This site is involved in rapid, long-range, outer-sphere electron transfer [12]. This reactivity has been related to the ground state wavefuction of the Cu(II) site, which is highly covalent thanks to a strong interaction with the thiolate sulphur of a cysteine ligand. The resulting HOMO for the Cu(II) site is quite delocalized and about half of the formal d vacancy is filled by charge transfer from the ligands [13]. The crystal structure is also highly refined [14].

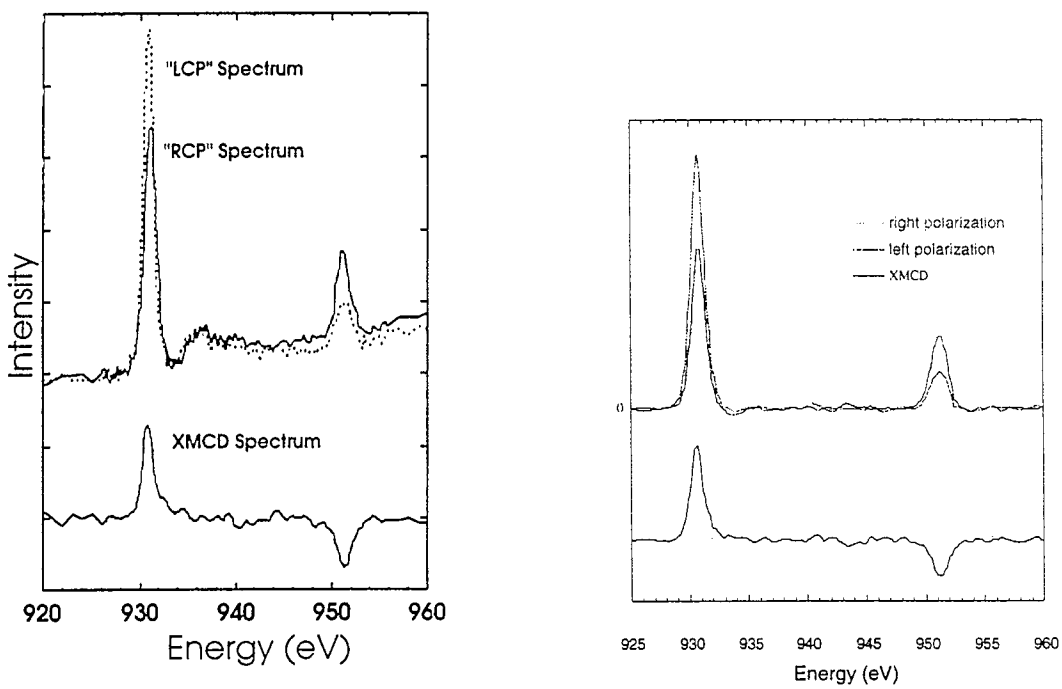

Fig. 4. (Left) L-edge XMCD spectra of Cu^{2+} plastocyanin at 4.2 K and 6 T: (top) spectra using left and right 75% circularly polarized light and (bottom) XMCD. (Right) Same spectra, recorded at 0.4 K and 2 T. The sample was treated with $K_3[Fe(CN)_6]$ to oxidize residual Cu^{1+} plastocyanin.

As shown in Fig. 4, a strong XMCD effect was observed for Cu^{2+} plastocyanin at 4.2K and 6 T. This spectrum is a nice example of the paramagnetic selectivity of XMCD — notice how the residual diamagnetic Cu(I) in this sample contributes to absorption near 936 eV, but does not affect the XMCD signal. More recently, we recorded the XMCD at 2 T with our new dilution refrigerator system and a 30-element detector. A magnetization curve found a temperature of 400 mK. The baseline stability has been improved by using the oxygen Kα signal as an internal I_0.

Thanks to the improvement in XMCD statistics and baseline quality, we are now able to test the application of the XMCD sum rules to bioinorganic systems. As discovered by Thole and detailed elsewhere in this volume, the integrated XMCD intensity is related to the orbital angular momentum at the absorbing site, while the spin angular momentum is more closely related to the integrated absolute value of the XMCD effect.

These sum rules have been tested and applied on a number of metallic and mixed multilayer systems [15–18]. However, a number of factors make their validity questionable for fluorescence-detected spectra in dilute bioinorganic systems. Experimentally, there is concern about how well the fluorescence-detected spectrum approximates the true absorption spectrum. The fluorescence yield may vary across the L-edge [19], and there may be significant angular variation in the emission [11] Theoretically, there is always the question of how well the number of holes is known, and the approximation that $\langle T_z \rangle = 0$ is often not valid [20]. For the moment, we have temporarily suspended these concerns and applied the sum rules to blue copper, as well as Ni^{2+} doped MgO, and the Fe^{2+} and Fe^{3+} centers in reduced and oxidized rubredoxin. As shown in Fig. 5, the results are not completely unreasonable, despite the number of valid concerns. Further work is needed to see how useful XMCD sum rule analysis will be for bioinorganic electronic structure analysis.

9. XMCD of coupled 2Fe systems

One of the features of XMCD that is especially

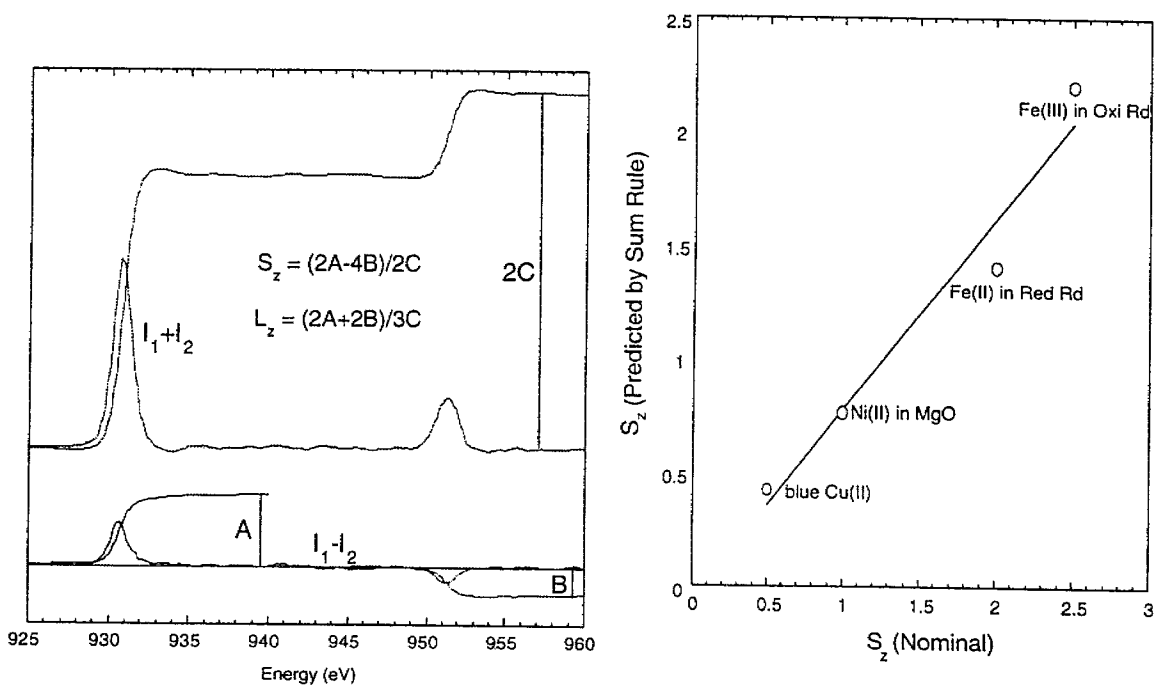

Fig. 5. (Left) Integrations for application of sum rules to Cu^{2+} plastocyanin XMCD (Right) Trends in $\langle S_z \rangle$ and $\langle L_z \rangle$ calculated from sum rules.

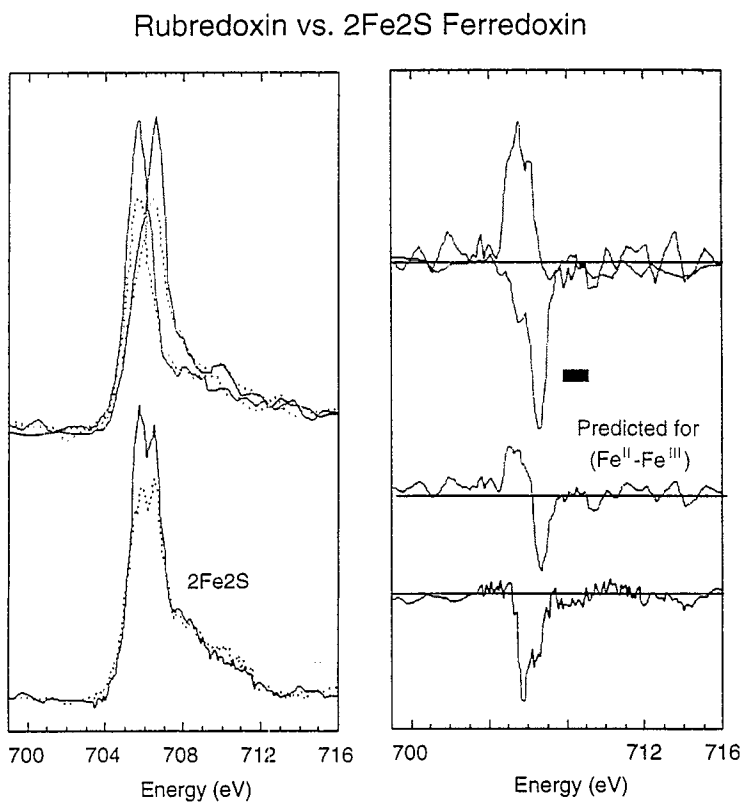

Fig. 6. (Left) top — Spectra for reduced (green) and oxidised (red) rubredoxin in different polarisations; bottom — 2Fe–2S spectra. (Right) top — XMCD spectra for reduced (green) and oxidised (red) rubredoxin; the reduced spectrum has been inverted to represent the fact that the Fe^{2+} site is antiferromagnetically coupled to the Fe^{3+} site; middle — an empirical XMCD spectrum generated by adding the normal oxidised and inverted reduced rubredoxin XMCD; bottom — observed 2Fe–2S XMCD.

attractive for bioinorganic studies is the prospect of investigating local spin orientations in coupled metal clusters. In theory, the sign of the XMCD should reveal the orientation of $\langle S_z \rangle$ for individual metal centres with respect to the incoming beam. This feature was originally used to investigate local moments in GdFe garnets [21], and has more recently been used to study magnetic multilayers. We have attempted to confirm this spin-orientation capability for bioinorganic systems by comparing the XMCD of an antiferromagnetically coupled $Fe^{2+}Fe^{3+}$ system with spectra for similar mononuclear sites.

Rubredoxins are small electron transfer proteins which contain single iron atoms co-ordinated by a distorted tetrahedron of cysteinyl sulphur ligands. 2Fe–2S ferredoxins are small ~13–14 kDa proteins which contain 2 tetrahedral Fe sites bridged by 2 inorganic sulphide residues [22]. As shown in Fig. 6, both oxidised Fe^{3+} and reduced oxidised Fe^{2+} *Pyrococcus furiosus* rubredoxin show strong XMCD effects. The oxidised rubredoxin Fe site is a $S = 5/2$ system, while the reduced protein is $S = 2$. The conventional view is that similar high-spin Fe sites are antiferromagnetically coupled in the 2Fe–2S ferredoxin proteins to yield an $S_{tot} = 1/2$ paramagnet in the mixed valent form [22].

Although the absorption spectrum for human mitochrondrial 2Fe–2S protein seems consistent with the summation of reduced and oxidised contributions, the XMCD does not show the expected bipolar signal. There is significant XMCD intensity in both the Fe^{2+} and Fe^{3+} regions, which is different from a recent report that found no intensity in the Fe^{2+} region of a related protein [23]. Since the

coupling constant J is thought to be on the order of $-100\ cm^{-1}$, the applied magnetic field should not be strong enough to overcome the antiferromagnetic interaction between the two metals.

At the moment, we cannot explain the puzzling XMCD behaviour of this relatively simple system, and progress in this area is needed before tackling more complex metalloprotein clusters. Of possible relevance is the observation that all of the NMR hyperfine signals of human ferredoxin exhibit Curie-type behaviour, whereas in plant ferredoxins half of the cysteine hyperfine signals exhibit Curie behaviour and the other half exhibit anti-Curie behaviour [24]. Perhaps the electronic structure of the human ferredoxin is more complex than we originally assumed.

10. The future

The near future should see substantial improvements in our experimental capabilities. An elliptical undulator beamline is under construction which will deliver far more flux at high resolution. A new generation of ultralow temperature microcalorimeters and tunnel–junction detectors offers the promise of much lower detection limits for dilute samples. Additional interesting XMCD effects might be observed at very high magnetic fields, and a 17 T system for such experiments is under consideration. Although it is no longer fashionable to name spectroscopies after individuals, in many respects XMCD should be considered Thole spectroscopy.

Acknowledgements

We thank the following collaborators for useful theoretical discussions and interest: C.T. Chen, F.M.F. de Groot, George Sawatzky, E.I. Solomon and the late J.C. Fuggle. Past workers on the XMCD project include Jason Christiansen, Xin Wang, Marie-Anne Arrio, Jie Chen, Gang Peng Jan van Elp, and Simon George. Model compounds have been provided by Terry Collins, Julie Kovacs, Michelle Millar, Pradip Mascharak, and Larry Que. Metalloenzyme samples were provided by Mike Adams (rubredoxin), Bin Xia and John Markeley (human ferredoxin) Daulat Patel (hydrogenase), Manoj Kumar and Steve Ragsdale (*C. thermoaceticum* CODH) and Nate Spangler and Paul Ludden (*R. rubrum* CODH).

This work was supported by the National Institutes of Health, grant GM-44380, the National Science Foundation, grants DIR-9105323 and DMB-9107312, and by the Department of Energy, through the Office of Health and Environmental Research. The Advanced Light Source, the National Synchrotron Light Source and the Stanford Synchrotron Radiation Lab are supported by the Department of Energy.

References

[1] F.M.F. de Groot, J.C. Fuggle, B.T. Thole, G.A. Sawatzky, Physical Review B 41 (1990) 928.
[2] B.T. Thole, R.C. Cowan, and G.A. Sawatzky, Physical Review B 31 (1985) 6856–6858.
[3] S.W. Ragsdale, M. Kumar, Chemical Reviews 96 (1996) 2515–2539.
[4] S.P.J. Albracht, Biochimica Et Biophysica Acta—Bioenergetics 1188 (1994) 167–204.
[5] A. Volbeda, M.H. Charon, C. Piras, E.C.Hatchikian, M. Frey and J.C. Fontecillacamps, Nature 373 (1992) 580–587.
[6] G. van der Laan, B.T. Thole, G.A. Sawatzky, M. Verdaguer, Physical Review B 37 (1988) 6587.
[7] C.P. Wang, R. Franco, J.J.G. Moura, I. Moura, E.P. Day, Journal of Biological Chemistry 267 (1992) 7378–7380.
[8] J. van Elp, G. Peng, Z.H. Zhou, M.W.W. Adams, N. Baidya, P.K. Mascharak, S.P. Cramer, Inorganic Chemistry 34 (1995) 2501–2504.
[9] G. van der Laan, B.T. Thole, Physical Review B 42 (1990) 6670–6674.
[10] G. van der Laan, B.T. Thole, Physical Review B 43 (1991) 13401–13411.
[11] M. van Veenendaal, J.B.M. Goedkoop, B.T. Thole, Physical Review Letters 77 (1996) 1508–1511.
[12] E.L. Gross, Photosynthesis Research 37 (1993) 103–116.
[13] S.J. George, M.D. Lowery, E.I. Solomon, S.P. Cramer, Journal of the American Chemical Society 115 (1993) 2968–2969.
[14] B.A. Fields, H.H. Bartsch, H.D. Bartunik, F. Cordes, J.M. Guss and H.C. Freeman, Acta Crystallographica Section D–Biological Crystallography 50 (1994) 709–730.
[15] C.T. Chen, Y.U. Idzerda, H.J. Lin, N.V. Smith, G. Meigs, E. Chaban, G.H. Ho, E. Pellegrin, F. Sette, Physical Review Letters 75 (1995) 152–155.
[16] W.L. O'Brien, B.P. Tonner, G.R. Harp, S.S.P. Parkin, Journal of Applied Physics 76 (1994) 6462–6464.

[17] J. Stohr, H. Konig, Physical Review Letters 75 (1995) 3748–3751.
[18] J.G. Tobin, K.W. Goodman, G.J. Mankey, R.F. Willis, J.D. Denlinger, E. Rotenberg, A. Warwick, Journal of Vacuum Science and Technology B 14 (1996) 3171–3175.
[19] F.M.F. de Groot, M.-A. Arrio, P. Sainctavit, C. Cartier, and C.T. Cheng, Solid State Communications 92 (1994) 991–995.
[20] P. Sainctavit, M.A. Arrio, C. Brouder, Physical Review B 52 (1995) 12766–12769.
[21] P. Rudolf, F. Sette, L.H. Tjeng, G. Meigs, and C.T. Chen, Journal of Magnetism and Magnetic Materials 109 (1992) 109–112.
[22] L. Noodleman, C.Y. Peng, D.A. Case, J.M. Mouesca, Coordination Chemistry Reviews 144 (1995) 199–244.
[23] J. van Elp, G. Peng, Z.H. Zhou, S. Mukund et al., Physical Review B 53 (1996) 2523–2527.
[24] L. Skjeldal, J.L. Markley, V.M. Coghlan, L.E. Vickery, Biochemistry 9078 (1991) 9078–9083.